Journal of
Applied Crystallography
ISSN 0021-8898

Received 26 May 2006
Accepted 29 August 2006

An instrument for time-resolved and anomalous simultaneous small- and wide-angle X-ray scattering (SWAXS) at NSRRC

Ying-Huang Lai,[a] Ya-Sen Sun,[a] U-Ser Jeng,[a]* Jhih-Min Lin,[b] Tsang-Lang Lin,[b] Hwo-Sheunn Sheu,[a] Wei-Tsung Chuang,[a] Yu-Shan Huang,[a] Chia-Hung Hsu,[a] Ming-Tao Lee,[a] Hsin-Yi Lee,[a] Keng S. Liang,[a] Andre Gabriel[c] and Michel H. J. Koch[d]

[a]National Synchrotron Radiation Research Center, 101 Hsin-Ann Road, Hsinchu Science Park, Hsinchu 30076, Taiwan, [b]Department of Engineering and System Science, National Tsing Hua University, Hsinchu 30013, Taiwan, [c]D2L, Le Carlin, F-38500 Saint Cassien, F-38500 Saint Cassien, France, and [d]European Molecular Biology Laboratory, Hamburg Outstation, EMBL c/o DESY, D-22603 Hamburg, Germany. Correspondence e-mail: usjeng@nsrrc.org.tw

A SWAXS (small- and wide-angle X-ray scattering) instrument was recently installed at the wiggler beamline BL17B3 of the National Synchrotron Radiation Research Center (NSRRC), Taiwan. The instrument, which is designed for studies of static and dynamic nanostructures and correlations between the nano (or *meso*) structure (SAXS) and crystalline structure (WAXS), provides a flux of 10^{10}–10^{11} photon s^{-1} at the sample at energies between 5 and 14 keV. With a SAXS area detector and a WAXS linear detector connected to two data acquisition systems operated in master–slave mode, the instrument allows one to perform time-resolved as well as anomalous scattering measurements. Data reduction algorithms have been developed for rapid processing of the large SWAXS data sets collected during time-resolved measurements. The performance of the instrument is illustrated by examples taken from different classes of ongoing projects: (i) time-resolved SAXS/WAXS/differential scanning calorimetry (DSC) with a time resolution of 10 s on a semicrystalline poly(hexamethylene terephthalate) sample, (ii) anomalous SAXS/WAXS measurements on a nanoparticulate PtRu catalyst, and (iii) grazing-incidence SAXS of a monolayer of oriented semiconductor quantum wires, and humidity-controlled ordering of Alamethicin peptides embedded in an oriented lipid membrane.

© 2006 International Union of Crystallography
Printed in Great Britain – all rights reserved

1. Introduction

Small-angle X-ray scattering (SAXS) is one of the most popular techniques in the nanosciences, as illustrated by the strong demand for SAXS beamtime at synchrotron radiation facilities worldwide. The increase in spectral brilliance of these sources over the years has considerably broadened the range of application of the technique. Measurement strategies integrating complementary tools such as SAXS, WAXS, DSC or infrared spectroscopy in a single instrument allowing simultaneous measurements have also opened new possibilities for studying correlations between phenomena occurring at different length scales (atomic to nano and *meso* scales), as well as correlations between structures and physical or optical properties. These correlations often provide crucial information for improving nanostructure-based devices. Following the trend at a number of facilities where SAXS instruments that integrate different methods are already operational [X33(D1/2) at the EMBL in HASYLAB (Rapp *et al.*, 1995), BL4-2 at the SSRL (Tsuruta *et al.*, 1998), X27C, NSLS, BNL (Chu & Hsiao, 2001), ID02 (Narayanan *et al.*, 2001), ID13 (Riekel, 2003), DUBBLE (Bras & Ryan, 1998) at the ESRF, BL5.2 at Elettra (Amenitsch *et al.*, 1995), and BL-45XU at SPring-8 (Fujisawa *et al.*, 2000), to name a few], an instrument capable of performing simultaneous SAXS, WAXS and DSC measurements on soft matter and nanoparticles was recently built at beamline BL17B3 of the National Synchrotron Radiation Research Center (NSRRC). Although time-resolved anomalous SAXS/WAXS experiments can also be done on this new instrument, the potential of this approach has not yet been fully exploited.

The present report gives a detailed description of the layout of the instrument as well as of its data acquisition system and data processing algorithms. The performance of the instrument is illustrated by: (i) simultaneous SWAXS/DSC measurements with a time resolution of 10 s on a semicrystalline poly(hexamethylene terephthalate) (PHT) sample, (ii) anomalous SWAXS measurements on a nanoparticulate PtRu catalyst, and (iii) grazing-incidence SAXS (GISAXS) studies of oriented semiconductor quantum wires and of

humidity-dependent ordering of Alamethicin peptides in an oriented lipid membrane.

2. Instrument

2.1. Photon source and beamline optics

The 13 mrad horizontal radiation fan of the 25-pole 1.8 T wiggler located at beam port 17 of the NSRRC is divided over three stations for powder diffraction (17A), general X-ray scattering (17B), and EXAFS (17C). Beamline 17B, which uses the central 4 mrad of the wiggler radiation, delivers beam to the eight-circle general purpose diffractometer at the 17B1 station or to the SWAXS instrument at the BL17B3 endstation. The optical layout of the front end of beamline 17B, shown in Fig. 1, includes a graphite filter, slits and a water-cooled rhodium-coated collimating mirror (CM). After the CM, the beam can be focused by a Si(111) double-crystal monochromator (DCM). The first crystal is flat, whereas the second one can be sagittally bent. The horizontally focused beam (2:1 demagnification) is focused vertically to the centre of the diffractometer in the 17B1 hutch by a spherical mirror (FM). For the SWAXS endstation, located downstream from the 17B1 hutch with the sample position at ~36.0 m from the source, the sagittal focusing of the DCM is not used to obtain the best possible angular resolution. With the optics outlined above, a flux of 10^{10}–10^{11} photons s^{-1}, covering the energy range between 5 and 14 keV with an energy resolution of $\sim 2 \times 10^{-4}$, was measured with a 0.5 mm diameter beam at the sample position of the SWAXS instrument in the 17B3 hutch. With these specifications it is possible to record anomalous SWAXS from systems containing Pt, Au, and/or other elements with characteristic K or L absorption edges in this energy range.

2.2. Instrument layout

From the source to the detector, the instrument (Fig. 2) consists of a collimation system, a laser alignment system, an attenuator, monitors, a sample stage, beamstop and detector system. The collimation system includes a set of slits (S1) and two sets of pinholes. The slits and the first pinhole (P1), which are 4 m apart, are used to define the beam, whereas the second pinhole (P2), which always has a larger diameter than P1, is a guard against parasitic scattering. Pinholes are made in a 1 mm thick tantalum (Ta) disk, with a choice of diameters (0.4, 0.5, 0.6, 0.8, 1.0 or 1.2 mm). The laser system provides rapid and efficient alignment of the sample and beamstop. With 20 channels of different metal (Al, Cu, Bi) foil thicknesses, the attenuator can reduce the intensity of the incident beam when measuring strong scatterers or sample transmission, which is obtained by taking the ratio of the intensities of the highly attenuated direct beam measured with and without sample. The incident beam flux is monitored by an NaI scintillation counter located after the first pinhole and is used for flux normalization in the data reduction routines (see below). A Kapton reflector and a second NaI detector behind P2 are used to align this pinhole and are removed from the beam path after alignment. An additional slit system is attached to each of the two pinhole systems to cut down the beam size in GISAXS measurements. The sample stage is equipped with motorized rotations, translations and tilting for alignment. The sample cell for bulk or solution samples of various sizes with up to 5 mm thickness and 5 mm diameter was designed to perform SWAXS measurements, with the temperature controlled by a silicon-oil based cooler (253–473 K) and/or an oven with heating rods (303–573 K).

The entrance of the vacuum pipe between sample and detector (254 mm diameter, with a variable length between 400 and 2750 mm) is 20 mm wide and 100 mm long and allows WAXS data collection using a 20 cm linear LC delay line gas proportional detector (Gabriel, 1977). The linear detector can be translated along a 1 m long and 10 mm wide aperture at the top of the pipe and can be rotated. A 20 cm long motorized slit in front of the detector defines its acceptance. The detector can cover a wide range of wavevector transfer $Q = 4\pi \sin\theta/\lambda$, where λ is the wavelength and 2θ the scattering angle, by adjusting the sample-to-detector distance and, to a lesser extent, the wavelength of the incident beam.

The exit window of the post-sample vacuum pipe is sealed by a 200 × 200 mm position-sensitive gas proportional area detector with delay line readout. A motorized beamstop, in front of the detector, blocks the direct beam, and for GISAXS measurements an additional beamstop can be added to block the strong specular beam from the sample substrate. Between the area detector and the beamstops there is a 20 mm gap allowing the insertion of an imaging plate to record SAXS scattering patterns with a large dynamic range. The vacuum

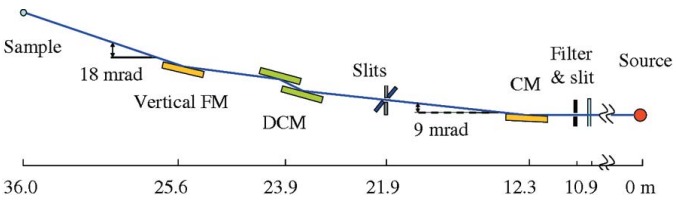

Figure 1
Optical layout of beamline 17B at the NSRRC. The sample position of the SWAXS instrument is at ~36 m from the source.

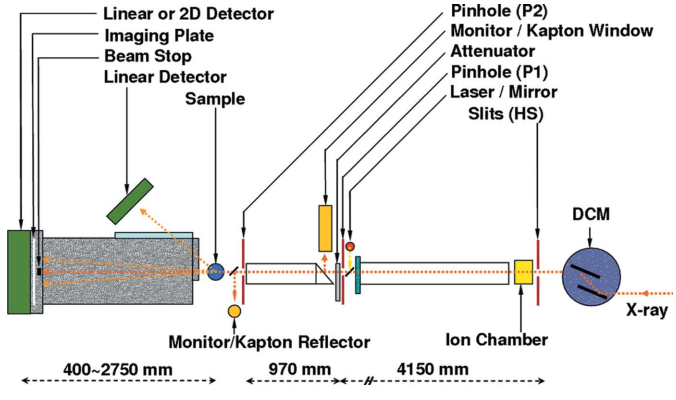

Figure 2
Schematic view of the SWAXS instrument at BL17B3. DCM: double crystal monochromator.

pipe is positioned on a fully motorized optical table and can be moved vertically and horizontally, as well as tilted and rotated. Together with the adjustments of sample-to-detector distance and wavelength, this gives great flexibility in recording scattering patterns in the optimal Q range for the specific experiments. If required, the SAXS and WAXS Q ranges can be made to overlap in a single configuration of the instrument.

2.3. Data acquisition system for simultaneous SWAXS measurements

For SWAXS data collection, the two detectors are connected to two PC-based data acquisition systems operated in master–slave mode, where the SAXS system is master and the WAXS system slave. The minimum time resolution depends on the flux, the scattering intensity of the sample and the efficiency of the area detector. The one-to-one frame correspondence between the time-dependent SAXS and WAXS data provides exact time correlations between the two measurements. Details of the data acquisition system have been described elsewhere (Shang *et al.*, 2004).

2.4. Instrument calibration and data reduction

Calibration of the WAXS Q axis is done using an analytical formula. For this purpose, three pixels, n_1, n_2 and n_3, of the detector are associated with three Q values (Q_1, Q_2 and Q_3) corresponding to arbitrary known diffraction peaks of a standard sample such as silicon and/or sodalite, with scattering angles θ_1, θ_2 and θ_3. Given the inclination angle α, three relationships can be constructed,

$$L\cos\alpha - L\sin\alpha\cot(\alpha+\theta_i) = n_i + n_{\rm off} \quad (i=1,2,3),$$

where L is the base length and $n_{\rm off}$ the channel offset, as illustrated in Fig. 3.

These equations are readily solved for the three parameters L, α and $n_{\rm off}$. The scattering angle or Q value of each detector pixel can then be expressed in terms of $n_1(Q_1)$, $n_2(Q_2)$ and $n_3(Q_3)$.

Fig. 4 illustrates the WAXS profile of sodalite, measured with 10 keV photons and calibrated with its own three peaks located at 2.64, 3.00 and 3.31 Å^{-1}. The WAXS profile overlaps well with that measured using the BL17A powder diffractometer. The deviations between every two corresponding peak positions in the two profiles are all less than 0.3%, which validates the Q-calibration method developed. When the data reduction algorithm using the three detector pixels calibrated with sodalite is applied to the pattern of a poly(trimethylene terephthalate) (PTT) sample measured with 8 keV photons with the same detector configuration, the resulting WAXS profile also matches that of the same sample measured at BL17A, as illustrated in the inset of Fig. 4.

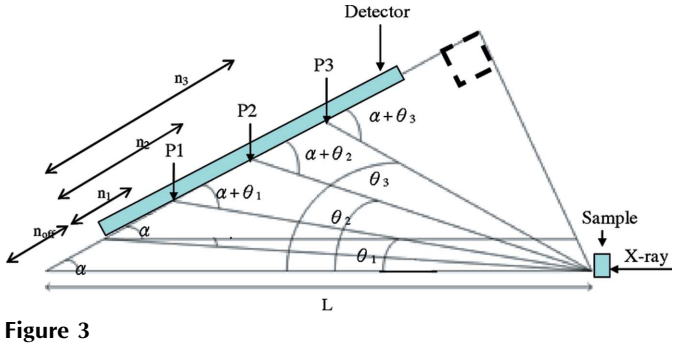

Figure 3
Scattering geometry for the WAXS linear detector, with the base length L and detector offset channel $n_{\rm off}$.

The Q-calibration algorithm has been incorporated into a WAXS data reduction routine developed for processing the large time-resolved WAXS data sets. The data reduction routine corrects for (i) detector electronic noise, (ii) background scattering, (iii) incoming flux, and (iv) angle-dependent sample path length, and converts the pixel coordinates to Q values. The sensitivity of the detector and the airpath-length-dependent absorption are corrected by dividing the WAXS spectrum of the sample, pixel by pixel, by the fluorescence of a metal sheet (*e.g.* iron for 8 keV photons) irradiated by the same beam with the same detector configuration. These corrections are especially important for anomalous scattering measurements for composition determination.

Similarly, SAXS data reduction routines were developed to reduce the two-dimensional scattering patterns collected with the area detector into one-dimensional $I(Q)$ profiles, and convert the scattering intensity to absolute scale (*i.e.* scattering cross section per unit sample volume). In this case, silver behenate and high-density polyethylene are used for Q calibration and absolute intensity scaling, respectively (Lai *et al.*, 2005). The SAXS data reduction routine corrects for (i) detector electronic noise, (ii) detector pixel sensitivity, (iii) background scattering, (iv) sample transmission and thickness, and (v) incident flux. The large multiframe SAXS data sets

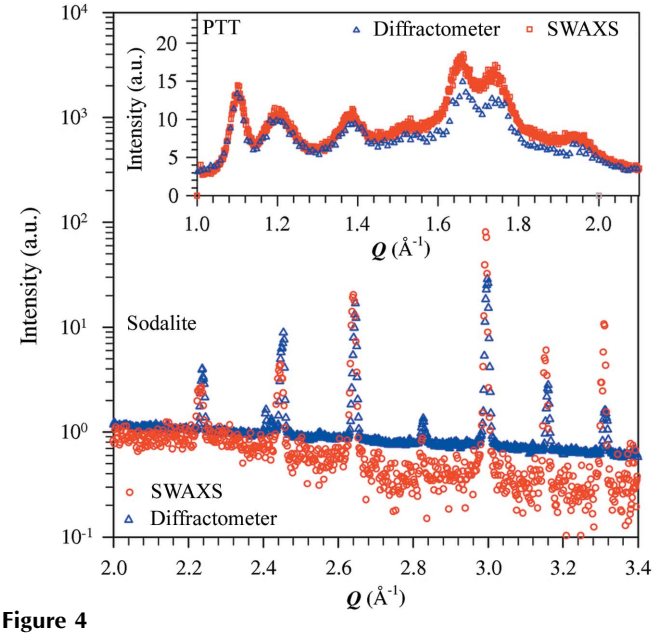

Figure 4
Comparison of the WAXS profiles of sodalite and of a polymer (PTT) sample (inset) measured, respectively, on the SWAXS instrument at BL17B3 using a linear detector and on the powder diffractometer at BL17A of NSRRC using an imaging plate for sodalite and an NaI point detector for PTT. No background was subtracted from the diffractometer data.

collected during time-resolved measurements can also be processed efficiently by the same data reduction procedure.

3. Performance

3.1. SWAXS/DSC measurement

The performance of the SWAXS instrument in time-resolved measurements is illustrated by the results obtained with a semicrystalline poly(hexamethyl terethphalate) (PHT) sample placed in a Mettler Toledo FP84 differential scanning calorimetry (DSC) cell with 2 mm diameter windows for X-rays. Fig. 5(*a*) presents the DSC scan for the sample recorded at 2.5 K min^{-1} after isothermal crystallization at 383 K. The SAXS and WAXS profiles recorded simultaneously are shown in Figs. 5(*b*) and 5(*c*) and illustrate the corresponding evolutions of the lamellar and crystalline structures of the sample. With a time resolution of 10 s, the first signs of crystal melting in the WAXS pattern are detected before any deterioration of the SAXS pattern (Chung *et al.*, 2006). The result reveals that the multiple melting peaks in the DSC trace can be attributed to sequential melting of the crystalline domains and the lamellar structure. A detailed analysis of these results will be reported elsewhere.

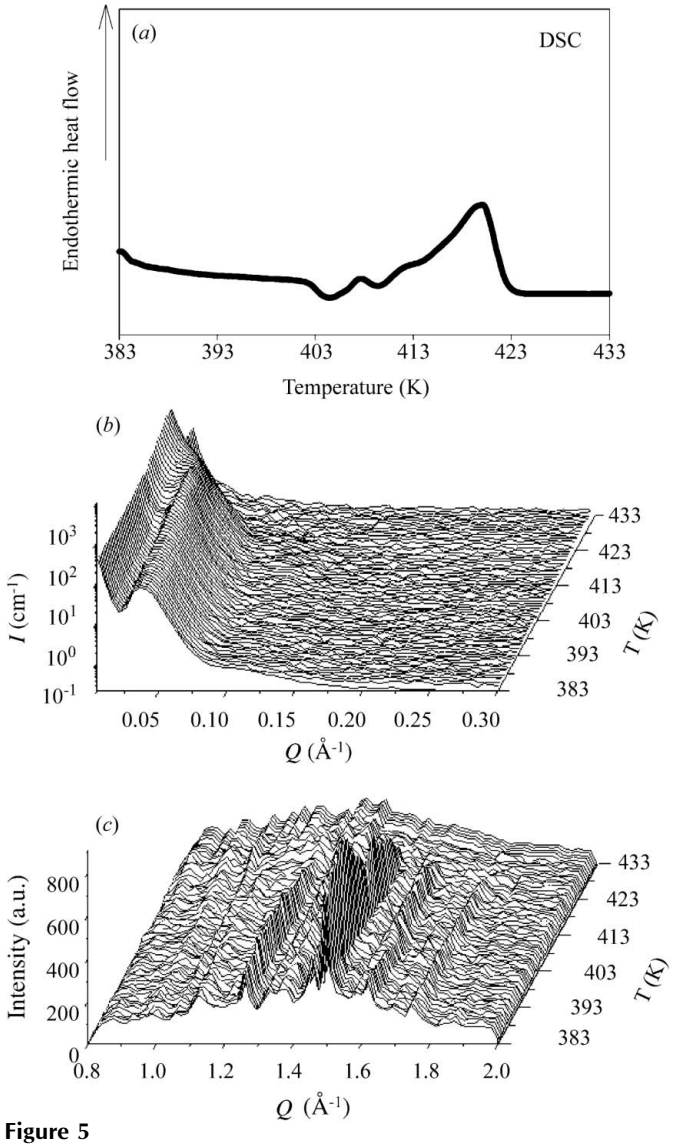

Figure 5
DSC thermogram (*a*) of PHT, melt-crystallized at 383 K for 120 min, and SAXS (*b*) and WAXS profiles (*c*) measured with a time resolution of 10 s during the DSC scan.

3.2. Anomalous SWAXS (ASWAXS) measurements

Time-resolved ASWAXS measurements under gas flow and temperature control are required, for example, for *in situ* studies of catalytic nanoparticles during isothermal annealing, aiming at obtaining a structure with higher catalytic efficiency. Before ASWAXS measurements, the WAXS profile obtained on the powder diffractometer at BL17A for the nanoparticles (Fig. 6) with a 1:1 Pt:Ru molar ratio, embedded in carbon powder, displays four face-centred-cubic (f.c.c.) crystalline peaks, which are shifted compared with those of pure Pt nanoparticles with an average diameter of 2.3 nm (Jeng *et al.*, 2005). Rietveld refinement indicates that the PtRu nanoparticles, which have a diameter of 2.0 ± 0.2 nm, have a Pt-like cubic phase ($Fm\bar{3}m$) with a cell dimension a = 3.912 (3) Å, which is smaller than that of the pure Pt nanoparticles (3.935 Å). The smaller cell dimension for the PtRu nanoparticles may be attributed to the existence of a PtRu alloy core or to the constraints due to a Ru shell which encloses the Pt core. ASWAXS can provide the composition of the nanoparticles as well as the structural information required to differentiate the core–shell structure from the alloy structure (Allen, 2005), as explained below.

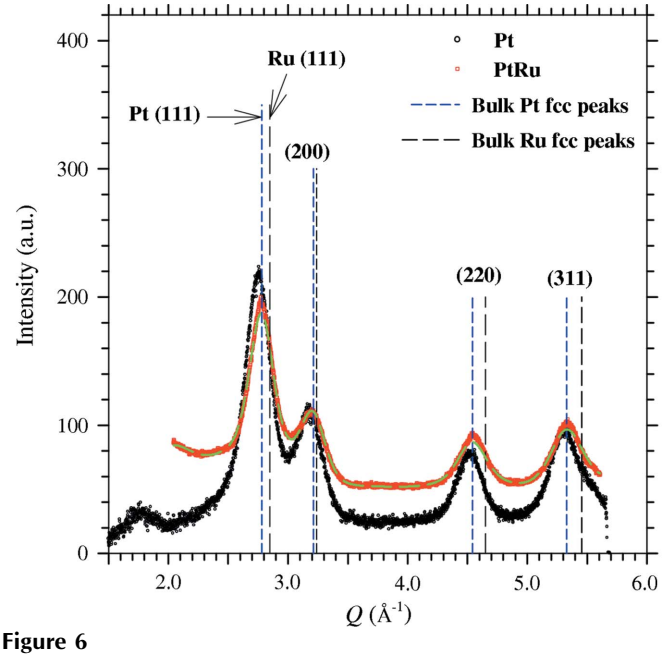

Figure 6
WAXS data for PtRu and Pt nanoparticles. The short-dashed and long-dashed vertical lines correspond to the positions of the four f.c.c. diffraction peaks of bulk Pt and Ru, respectively, with a cell dimension a = 3.920 Å for bulk Pt. The dashed curve obtained by Rietveld refinement overlaps well with the WAXS data of the PtRu nanoparticles.

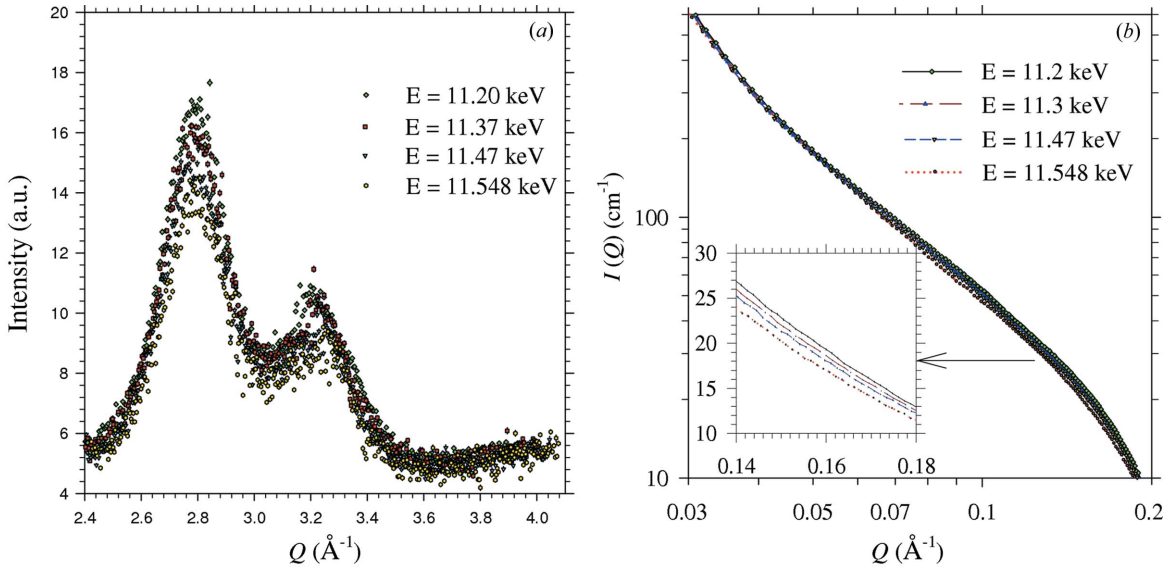

Figure 7
Selected AWAXS data (*a*) and ASAXS data (*b*) measured simultaneously at energies between 11.0 and 11.548 keV for the PtRu nanoparticles embedded in carbon black. The inset shows a zoomed-in view of the data.

Selected AWAXS and ASAXS profiles of oxidized PtRu nanoparticles measured simultaneously at energies between 11.2 keV and 11.548 keV are shown in Figs. 7(*a*) and 7(*b*). The intensity of the AWAXS profile gradually decreases as the energy approaches the $L_{\rm III}$ absorption edge of Pt (11.564 keV), clearly illustrating that the crystalline peaks are mainly associated with Pt (Haubold *et al.*, 1997). The ratio of the AWAXS peak intensities at two energies, E and E_0, can be calculated by $I_E/I_{E_0} = (f_E^2)/(f_{E_0}^2)$, with the complex atomic form factor f of the atoms that are responsible for the WAXS peak. Using E = 11.2 keV as a reference, the peak intensity ratios measured are consistent with that calculated using the energy-dependent f values of pure Pt. We thus conclude that the WAXS peaks are due to a crystalline structure containing nearly 100% Pt atoms. The smaller lattice constant of the crystalline structure in the PtRu nanoparticles is more likely due to the constraints from a Ru shell surrounding the Pt core than to a PtRu alloy core. The proposed core–shell structure can be further evidenced by the simultaneously measured ASAXS profiles in Fig. 7(*b*). There is a clear drop in intensity in the higher-Q region (0.1–0.2 Å^{-1}) as the energy approaches the $L_{\rm III}$ absorption edge of Pt, whereas the scattering profile at smaller Q values (0.03–0.05 Å^{-1}), corresponding to the scattering from the shell region and thus to a larger length scale, is insensitive to the beam energy. This result reveals that the contribution of the Pt atoms dominates the scattering of the core region, corresponding to the smaller length scale. On the other hand, the scattering of the large pores of carbon black, although dominating the scattering in the smaller Q region, is energy independent. Thus, we can still differentiate the energy-dependent contribution of the Ru shell of the nanoparticles from that of the pores, as evidenced previously by the ASAXS measurements performed at photon energies close to the Ru K-absorption edge at 22.117 keV (Lai *et al.*, 2005). Detailed structural information, including the size and composition of the Pt core and the thickness of the Ru shell, can, in principle, be obtained from the ASAXS data (Waseda, 2002). The combination of AWAXS and ASAXS yields, however, complementary structural information leading to a better understanding of the phenomena. In particular, *in situ* AWAXS/ASAXS can be used to monitor the possible core–shell inversion of the nanoparticles during isothermal annealing.

3.3. Grazing-incidence SAXS (GISAXS)

To probe the characteristic sizes and spatial correlations of oriented features confined to the sample surface, it is necessary to perform SAXS measurements in grazing-incidence geometry (Als-Nielsen *et al.*, 1994; Hsu *et al.*, 2004) and to rotate the sample azimuthally while keeping the incidence angle constant. A purpose-built sample stage consisting of two goniometers and a rotation stage allows one to align sample surfaces in the horizontal plane and to define an appropriately small angle of incidence. Such an assembly allows a convenient scan of GISAXS profiles during sample rotation for laterally anisotropic structures, such as monolayers of oriented quantum wires on semiconductor wafers. The grazing incidence angle relative to the sample surface can be accurately set within 0.005° and the beam size is defined using the slit systems described above. Typical incidence angles $\theta_{\rm in}$ are around 0.2° for glass substrates or silicon wafers and the sample size is about d = 30 mm along the incident beam. A beam size of $s = d\sin\theta_{\rm in} \simeq 100$ µm (vertical direction) thus covers the sample efficiently while preventing over-filling, which occurs when the footprint of the beam is larger than the sample size, thereby minimizing background scattering.

3.3.1. Oriented quantum wires. The performance of the instrument for GISAXS is illustrated by results obtained with a monolayer of oriented GaSb quantum wires on a GaSb

wafer, fabricated by low-energy ion bombardment. With an incidence angle close to the critical angle for total reflection of the GaSb wafer, the GISAXS pattern is obtained by in-plane rotation of the sample. When the orientation of the quantum wires is close to the direction of the incident beam, two in-plane scattering maxima, corresponding to the lateral ordering of the quantum wires, are observed as illustrated in Fig. 8(*b*). The spacing $d = 2\pi/Q_p$ between the quantum wires estimated from the position of these maxima (Q_p) is consistent with the value of 19.8 nm determined from the corresponding SEM image in Fig. 8(*a*).

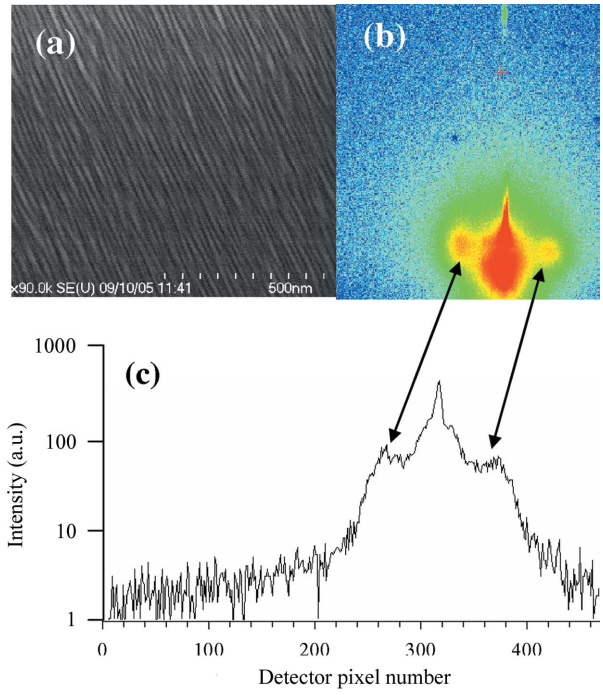

Figure 8
Scanning electron microscope (SEM) image of the oriented GaSb quantum wires (*a*). GISAXS pattern of the quantum wires recorded with the area detector (*b*) and corresponding profile taken across the two scattering maxima ($Q = 0.032$ Å^{-1}) in the pattern (*c*).

3.3.2. Humidity-dependent ordering of peptides in a lipid membrane. A sample cell with humidity and temperature control has been developed for GISAXS measurements on oriented lipid membranes. Results for a complex system of Alamethicin peptides embedded in an oriented lipid membrane of dioleoylphosphatidylcholine (DOPC) on a quartz plate are shown in Fig. 9. The data were taken for the liquid-crystal phase of the lipids (305 K) and relative humidities of $H = 35\%$ and 90%, respectively. In Fig. 9(*a*), the Bragg peak at $Q_z = 0.143$ Å^{-1} observed at $H = 35\%$ corresponds to the periodic structure of the lipid bilayers normal to the sample plane (in-depth direction) (Lee *et al.*, 2004). The additional scattering peak ($Q_z = 0.091$ Å^{-1}) appearing between the direct beam and the first Bragg peak of the lipid bilayers implies the existence of peptide ordering across the lipid bilayers. At higher (90%) humidity, the second lipid bilayer peak moves in the detector view (Fig. 9*b*) and the first peak moves to smaller Q values ($Q_z = 0.1251$ Å^{-1}), as a result of the bilayer swelling. Simultaneously, the scattering peak corresponding to the ordering of the peptide, also affected by the bilayer swelling, moves to a higher Q value ($Q_z = 0.1073$ Å^{-1}). The merging of the lipid and peptide ordering peaks in an environment of increasing humidity implies that the peptide can more easily adapt to the bilayer structure at higher humidity.

4. Concluding remarks

As illustrated above, the new SWAXS instrument for anomalous scattering and time-resolved measurements exhibits excellent performance for a wide range of applications. Rigorous data reduction routines are available to process the large SAXS and WAXS data sets collected in time-resolved SWAXS measurements. The instrument is being used for a variety of projects, including ongoing studies of the systems mentioned above. It is also planned to use *in situ* anomalous SWAXS to study the structural evolution of Al–Mg–Si alloys containing Cu (quaternary alloy). This type of material, which combines light weight and high mechanical strength, has recently attracted considerable attention both in academic and industrial research, especially for aerospace and automotive applications. Scattering measurements on protein solutions with concentrations of a few mg ml^{-1} are currently also under way, to study the structure of multidomain proteins which are too large to be resolved by NMR [*e.g.* the branched chain α-keto acid dehydrogenase (BCKD) complex], or the influence of temperature on the structure of proteins in solution.

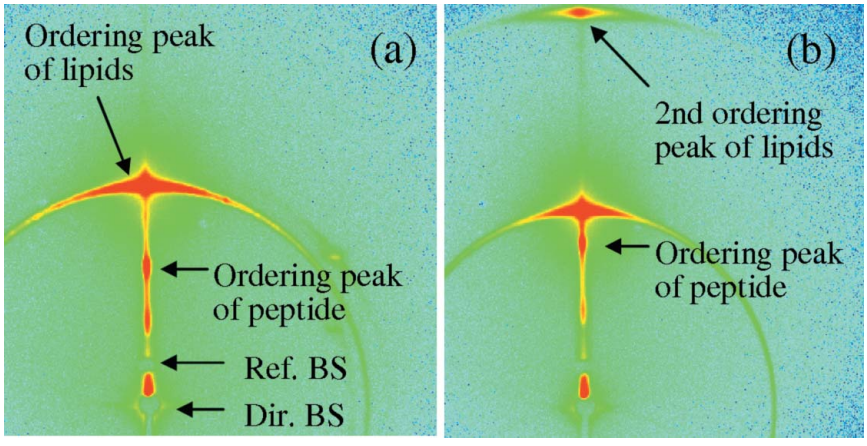

Figure 9
GISAXS patterns from Alamethicin peptides embedded in an oriented lipid membrane of DOPC at the liquid-crystal temperature were recorded with the area detector at relative humidities of $H = 35\%$ (*a*), with a first Bragg peak of lipids at $Q = 0.143$ Å^{-1}, and 90% (*b*), with a first Bragg peak at $Q = 0.128$ Å^{-1}. The intense direct beam and the specular beam from the sample substrate are blocked by two circular beamstops (BS).

We thank H. Liu and C.-H. Su for their help in setting up the instrument. The work was partially supported by the NSC under grant Nos. NSC-94-2112-M-213-003 and NSC-93-2b112-M-213-007.

References

Allen, A. J. (2005). *J. Am. Ceram. Soc.* **88**, 1367–1381.
Als-Nielsen, J., Jacquemain, D., Kjaer, K., Leveiller, F., Lahav, M. & Leiserowitz, L. (1994). *Phys. Rep.* **246**, 251–313.
Amenitsch, H., Bernstorff, S. & Laggner, P. (1995). *Rev. Sci. Instrum.* **66**, 1624–1626.
Bras, W. & Ryan, A. J. (1998). *Adv. Colloid Interface Sci.* **77**, 1–43.
Chu, B. & Hsiao, B. (2001). *Chem. Rev.* **101**, 1727–1761.
Chung, W.-T., Jeng, U., Sheu, H.-S., Hong, P.-D. & Lee, H.-Y. (2006). *Macromol. Res.* **14**, 45–51.
Fujisawa, T., Inoue, K., Oka, T., Iwamoto, H., Uruga, T., Kumasaka, T., Inoko, Y., Yagi, N., Tamamoto, M. & Ueki, T. (2000). *J. Appl. Cryst.* **33**, 797–800.
Gabriel, A. (1977). *Rev. Sci. Instrum.* **48**, 1303–1305.
Haubold, H.-G., Wang, X. H., Goerigk, G. & Schilling, W. (1997). *J. Appl. Cryst.* **30**, 653–658.
Hsu, C.-H., Jeng, U., Lee, H.-Y., Windover, D., Lu, T.-M. & Jin, C. (2004). *Thin Solid Films*, **472**, 323–327.
Jeng, U., Hsu, C.-H., Sun, Y.-S., Lai, Y.-H., Chung, W.-T., Sheu, H.-S., Lee, H.-Y., Song, Y.-F. & Liang, K. S. (2005). *Macromol. Res.* **13**, 506–513.
Lai, Y. H., Sun, Y. S., Jeng, U., Song, Y. F., Tsang, K. L. & Liang, K. S. (2005) *Nucl. Instrum. Methods B*, **238**, 205–213.
Lee, M.-T., Chen, F.-Y. & Huang, H. W. (2004). *Biochemistry*, **43**, 3590–3599.
Narayanan, T., Diat, O. & Boesecke, P. B. (2001). *Nucl. Instrum. Methods A*, **467–468**, 1005–1009.
Rapp, G., Gabriel, A., Dosiere, M. & Koch, M. H. J. (1995). *Nucl. Instrum. Methods A*, **357**, 178–182.
Riekel, C. (2003). *Nucl. Instrum. Methods B*, **199**, 106–111.
Shang, W., Robrahn, B., Golding, F. & Koch, M. H. J. (2004). *Nucl. Instrum. Methods A*, **530**, 513–520.
Tsuruta, H., Brennan, S., Rek, S. U., Irving, T. C., Tompkins, W. H. & Hodgson, K. O. (1998). *J. Appl. Cryst.* **31**, 672–682.
Waseda, Y. (2002). *Anomalous X-ray Scattering for Materials Characterization*. New York: Springer.